Algorithm Theoretical Basis Document
for
Sea Surface Temperature
Retrieval from INSAT-3D/3DR

S. No.	Product Name	Spatial Resolution	Temporal Resolution
1	3RIMG_L2B_SST	4 km	30 minutes
2	3RIMG_L3B_SST_DLY	4 km	Daily (00:00 – 23:30 hrs)
3	3DIMG_L2B_SST	4 km	30 minutes
4	3RIMG_L3B_SST_DLY	4 km	Daily (00:15 – 23:45 hrs)

1. Algorithm Configuration Information

1.1 Algorithm Name

Sea surface temperature (SST)

(Ref: IMD RFP Sec. 11.7)

1.2 Algorithm Identifier

3DIMG_L2B_SST, 3RIMG_L2B_SST

3DIMG_L3B_SST_DLY, 3RIMG_L3B_SST_DLY

1.3 Algorithm Specification

Version	Date	Prepared by	Description
1.0	13.01.2017	Rishi Kumar Gangwar and Pradeep Kumar Thapliyal	Revised ATBD
1.1	11.01.2018	Rishi Kumar Gangwar and Pradeep Kumar Thapliyal	Revised ATBD

2. Introduction

India successfully launched its advanced meteorological satellite INSAT-3DR on 26th September 2016 in the geostationary orbit at 74°E. The inheritance of this satellite has come from INSAT-3D satellite. Meteorological payloads onboard INSAT-3DR are a 6 channel Imager and a 19 channel Sounder mainly for atmospheric profiles, cyclone and monsoon monitoring, cloud motion vectors winds, rainfall estimation, floods/intense precipitation monitoring, snow cover detection, mesoscale studies etc. Apart from a 19 channel Sounder in INSAT-3D/3DR, the Imager has a split-window (TIR1/2), mid-IR (MIR) window, and shortwave IR (SWIR) channels in additions to earlier INSAT-3A/Kalpana VHRR. Details of the INSAT-3D/3DR Imager channels are given in Table-1. The spectral response functions (SRF) of TIR1 &2, MIR and WV bands of INSAT-3D are shown in figure (1) along with brightness temperature spectra of Infrared Atmospheric Sounding Interferometer (IASI) for a standard tropical atmosphere.

Table-1: Imager channels' characteristics

Band# (Name)	Wavelength(μm)	Resolution (km)	SNR or NEDT (K)
1 (VIS)	0.52 – 0.72	1	150:1
2 (SWIR)	1.55 – 1.70	1	150:1
3 (MIR)	3.80 – 4.00	4	0.27
4 (WV)	6.50 – 7.00	8	0.18
5 (TIR1)	10.3 – 11.2	4	0.10
6 (TIR2)	11.5 – 12.5	4	0.25

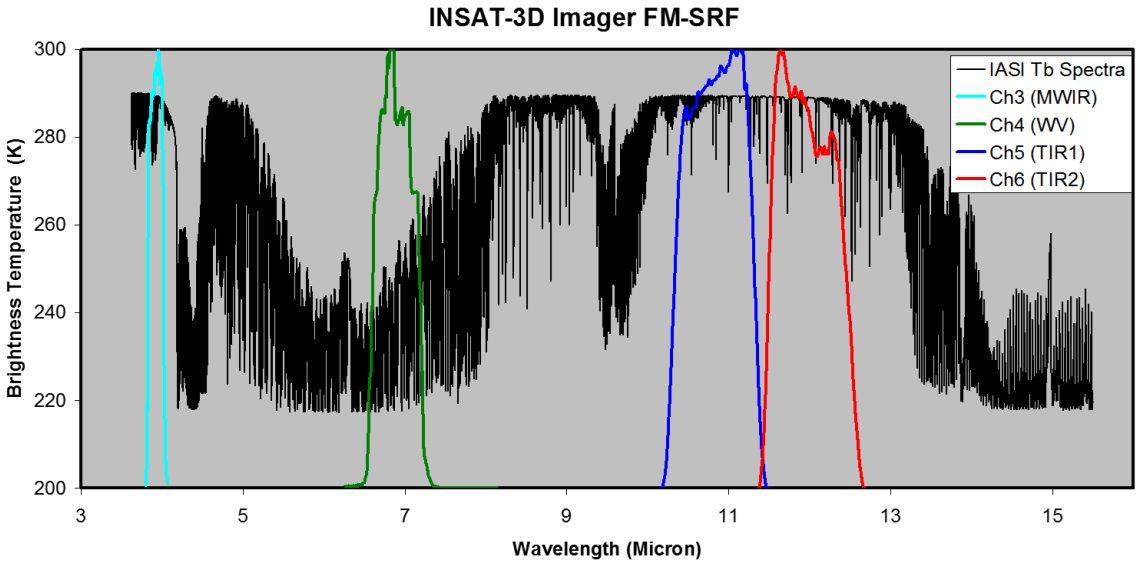

Fig. 1: Convolved SRFs of infrared channels of INSAT-3D Imager superimposed on IASI Tb spectra

Sea surface temperature is derived from the split thermal window channels (10.3-11.2μm, 11.5 – 12.5μm) during daytime and using additional midwave-IR window channel (3.8 – 4.0 μm) during nighttime over cloud free oceanic regions. The most important part of the SST retrieval from IR observations is the atmospheric correction. Especially over tropics, this atmospheric correction is dominated by the high variability in vertical distribution of the intervening atmospheric water

vapor. This correction is determined through suitable characterization of tropical atmosphere in the radiative transfer model to simulate the brightness temperatures of INSAT-3D/3DR channels and then generating the regression coefficients for SST retrieval. Details of the algorithm have been given in section 3.1.

2.1 Overview and background

This algorithm theoretical basis document (ATBD) describes the current operational algorithm for the retrieval of sea surface temperature from INSAT-3D/3DR Imager channels data. While effort has been made to make this document as complete as possible, it should be recognized that algorithm development is an evolving process. This document (V1.1) is a description of the revised algorithm for INSAT-3D/3DR sea surface temperature estimation as it currently exists, and is being delivered for inclusion in the INSAT-3D/3DR processing scheme.

Current research on the physics of the atmospheric transmission in the infrared, the processes at the ocean surface, and new information about the performance of the satellite will lead to periodic revisions of the algorithms. Also, the document may appear incomplete in places as research continues to improve our understanding of the processes at work. Subsequent revisions of the document will reflect new knowledge and, it is hoped, fill the gaps in what is reported here.

2.2 Objective

Development of complete application software package for derivation of SST using multi-channel Imager data from INSAT-3D/3DR.

2.3 Inputs

2.3.1 Static Data

Parameter	Resolution	Accuracy	Source
Land /Sea Mask	Pixel (~4 km)	1 pixel	USGS(available)
Climatological SST data	0.25 X 0.25 degree	0.5 K	Reynolds

2.3.2 Image and preprocessing data (Dynamic)

Parameter	Res.	Quant.	Accuracy	Source
Radiometric and geometric corrected gray count values of Channel-5 (10.2-11.3 μm)	Pixel	10 bit	-	Derived from raw data by DP
Radiometric and geometric corrected gray count values of Channel-6 (11.5-12.5 μm)	Pixel	10 bit	-	Derived from raw data by DP
Radiometric and geometric corrected gray count values of Channel-3 (3.8 – 4.0 μm)	pixel	10 bit	-	Derived from raw data by DP
Gray value to brightness temperature conversion lookup table	-	-	0.1 K	Derived by DP
Geolocation file	Pixel	-	1 pixel	Derived by DP
Satellite Zenith angle	Pixel			Derived by DP
Solar Zenith angle	Pixel			Derived by DP
Cloud Flag	Pixel	-	-	Cloud Routine

3. Algorithm Functional Specifications

3.1 Overview

3.1.1 Theoretical Background

Radiance from Earth's terrestrial emission peaks at around 10 μm and it has minimum attenuation by atmospheric gases. Hence in order to measure earth's surface temperature, space borne sensors are designed around this band (8-12μm). Still this band is not completely transparent. Atmospheric water vapour and CO_2 are the major constituents that attenuate the IR signal reaching at the top of the atmosphere in this wavelength band. Since CO_2 is a uniformly mixed gas, its effect can be taken care, but water vapour being highly variable in space and time needs additional information on total water content in the atmosphere (directly or indirectly). Retrieval of sea surface

temperature (SST) from thermal infrared window channels (10-12 μm) requires atmospheric correction arising due to attenuation of signal by intervening moisture. This correction is more in tropics during summer due to higher amount of atmospheric moisture loading (Barton 1983, Anding and Kauth 1970, Gohil et al 1994, Mathur & Agarwal 1991, 2002, Shenoy 1999). The radiative transfer simulation studies, carried out using diverse training profiles set, have shown that with proper characterization of water vapour in the atmosphere, a suitable algorithm can be developed for accurate SST retrieval (<0.7K) using split thermal window and mid IR thermal channels provided the sensor noise is of the order of 0.1K (Fig.2). The simplest of such algorithms assume that, for small cumulative amounts of water vapour, the atmosphere is sufficiently optically thin that the difference between the measured temperature in any band and the true surface temperature can be parameterized as a simple function of the difference between the measured temperatures in two bands with different atmospheric transmissions.

Linear algorithms like Multi Channel Sea Surface Temperature (MCSST) are based on a formula of the following form for the surface temperature T_s.

$$T_s = \alpha + \beta T_i + \gamma\left(T_i - T_j\right) \qquad (1)$$

where, the T_i's are the brightness temperatures in various bands for a given location and α, β and γ give the parametrized correction (Deschamps and Phulpin 1980, Llewellyn-Jones et al., 1984), or can be derived empirically from good composite sets of surface and satellite observations (Prabhakara, et al., 1974).

Although Eq. (1) is easy to implement, it does not permit correction for changes in air mass due to scan-angle. Llewellyn-Jones et al., (1984) develop a table from numerical simulations which permits modification of Eq. (1) into a form:

$$T_s = \alpha + \beta' T_i + \gamma'\left(T_i - T_j\right) + \delta(sec\theta - 1) \qquad (2)$$

where, θ is the satellite zenith angle and δ is an additional scan angle coefficient. This approach reduces the errors at large scan angles for moist atmospheres by more than 1K. This form, however, while improving the error behavior at large scan angles, does not adequately control the residual behavior at high temperatures.

A further generalization of this approach is to posit a non-linear structure for the SST estimator. For that a NLSST (non-linear SST) atmospheric equation uses the form:

$$SST = a_0 + a_1T_1 + a_2(T_1 - T_2) + a_3(T_1 - T_2).(T_1 - T_2) + a_4(sec\theta - 1).(T_1 - T_2) \quad (3)$$

where, *SST* is the satellite derived SST estimate, T_1 and T_2 are the brightness temperatures of INSAT-3DR thermal channels (TIR-1 and TIR-2). a_0, a_1, a_2, a_3 and a_4 are the retrieval coefficients estimated from the regression analysis using collocated simulated brightness temperatures and SST. The above equation (3) is currently operational at MOSDAC and IMD, Delhi.

The validation results of operational SST with in-situ and MODIS SST products has been presented in science team meeting of Group for High Resolution Sea Surface Temperature (GHRSST) held at China during 05-09 June, 2017. In the meeting the Science Team members suggested to drop the square term of the difference between brightness temperatures of TIR-1 & TIR-2, being used for correcting the atmospheric water vapour contamination. It was point out that if there is large noise in thermal channels, the square of their difference may result in large errors in SST, which was also observed on many occasions in the operational products. Therefore, based on the recommendations from GHRSST Science Team and subsequent validation analysis of the operational SST products, the SST retrieval algorithm has been modified to address this issue of large errors in SST due to non-linear WV correction term.

The revised algorithm follows Walton et al. (1998) for SST retrieval which has the following form:

Day-time:

$$SST = a_0 + a_1T_1 + a_2(\sec\theta - 1) + a_3T_{sfc}.(T_1 - T_2) + a_4(sec\theta - 1).(T_1 - T_2) \quad (4)$$

Night-time:

$$SST = a_0 + a_1T_3 + a_2(\sec\theta - 1) + a_3T_{sfc}.(T_1 - T_2) + a_4(sec\theta - 1).(T_1 - T_2) \quad (5)$$

where, T_3 is the brightness temperature of MIR channel. T_{sfc} is the a priori estimate of SST that can be taken from the climatology or from the forecast of the numerical weather prediction models. All other variables are same as in equation (3). The multiplication factor T_{sfc} is used to scale the correction factor due to atmospheric water vapor. We have also tried to experiment with the brightness temperature of TIR1 as a multiplying factor, which yields very similar result. However, in order to avoid occasional large noise in the TIR1 BT we retain T_{sfc} as the multiplying factor as in the original algorithm proposed by Walton et al. (1998).

3.1.2 Radiative Transfer Model

Since frequency bands and their spectral response functions of INSAT-3DR and INSAT-3D are almost similar, the transmission coefficients file of INSAT-3D required to simulate brightness

temperatures through PFAAST radiative transfer (RT) model can be used for simulating INSAT-3DR brightness temperatures. Therefore, we have simulated the brightness temperatures corresponding to INSAT-3DR thermal and mid-IR channels through PFAAST RT model. The atmospheric profiles and required surface variables has been taken from ECMWF diverse data set. The simulations have been performed for the clear atmospheres over oceanic region spanning from 0°E – 130°E and 60°S – 60°N only, and for satellite zenith angle from 0 to 60 degrees.

3.1.3 Cloud detection

In the present algorithm, the cloudy pixels are flagged using INSAT-3DR level-2 cloud mask product. In absence of the INSAT-3DR cloud mask product the cloudy pixels are detected through cloud mask routine based on threshold and spatial coherence techniques in visible, MIR and thermal bands. Threshold technique assumes that over oceans in Indian domain brightness temperature in thermal band (TIR-1) is greatly affected by the presence of clouds, resulting in decreased brightness temperature from cold cloud tops. Spatial coherence method is based on the assumption that SST is homogeneous in smaller spatial domain and sufficiently warmer than clouds; thus clouds can be identified where the scene brightness temperature has lower mean value or larger standard deviation. In addition to above the following thresholds criteria as described in ATBD of MODIS (Ackerman et al., 2006) cloud mask product have also been used.

During day time the reflection in MIR channels dominates over emission; therefore, in general MIR BT can be higher than TIR-1 BT by up to ~6K for clear-sky. However, for MIR channel the reflection coefficient is higher for cloud top than earth's surface. Hence the difference of TIR1 and MIR BTs becomes more negative for cloudy sky. The visible reflectance is very high for clouds as compared to earth's surface. Hence, higher visible albedo (>5 %) or reflectance corresponds to cloudy sky. During day-time (solar zenith angle < 80 degree) the following threshold criterion has been used to detect cloudy pixels:

$$T_1 - T_3 < -6.0 \;\&\; (visible\ count > 70\ or\ albedo > 5)$$

where, T_1 and T_3 are the brightness temperatures of TIR-1 and MIR channels of INSAT-3D/3DR, respectively.

During night there is no solar reflection at MIR wavelength hence satellite measures only emitted radiation. Since cloud emissivity is lower for MIR as compared to TIR-1 wavelength, the brightness temperature corresponding to MIR will be smaller than that of TIR-1 BT for cloudy pixels. Hence, during night-time (solar zenith angle >= 80 degree) the following threshold is used to mask the cloudy pixels:

$$T_1 - T_3 > -1.0$$

SST is computed only over clear oceanic regions.

3.1.4 Error Analysis

A simulation based sensitivity study of noise in TIR-1 & TIR-2 channels' BTs on the SST retrieval has been carried out to analyze the errors in the retrieved SST. The simulations have been performed through PFAAST radiative transfer model using atmospheric profiles from ECMWF diverse training dataset for INSAT-3D spectral response functions. The following figure (2) is showing the impact of noise in both the channels on the errors in the retrieved SST. From the figure it can be clearly pointed out that if both the channels have uncertainty of 0.1K, the theoretical error in retrieved SST would be ~ 0.7K. If uncertainty in both the channels is ~0.05K the minimum possible error in the retrieved SST would be 0~.55K.

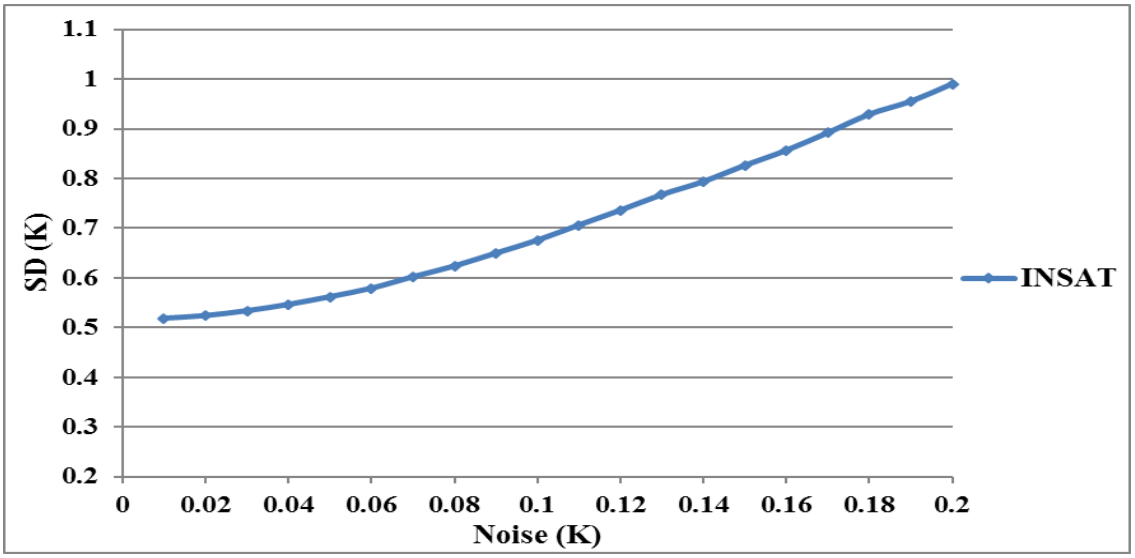

Fig. 2: Sensitivity of total noise in the retrieval of SST from INSAT-3D Imager

It can also be inferred from the figure (2) that using split-window channels the best possible SST accuracy of 0.5K could be achieved. For getting better than 0.5K accuracy, one should opt other atmospheric WV correction techniques as used in ATSR mission which gives approximately 0.3K (Mutlow, et al., 1994; Minnett, 1988; Barton, et al., 1993) errors in retrieved SST. In ATSR dual-view configuration has been used to correct the atmospheric WV. The Superiority of the dual-view

algorithm over single-view split-window algorithm lies in the fact that use of the cleaner window for atmospheric correction using second view with larger path-length reduces the uncertainty that arises in the split window algorithm due to larger uncertainties in the attenuation in the second split-window channel due to highly variable atmospheric water vapor.

3.2 Algorithm Flowchart

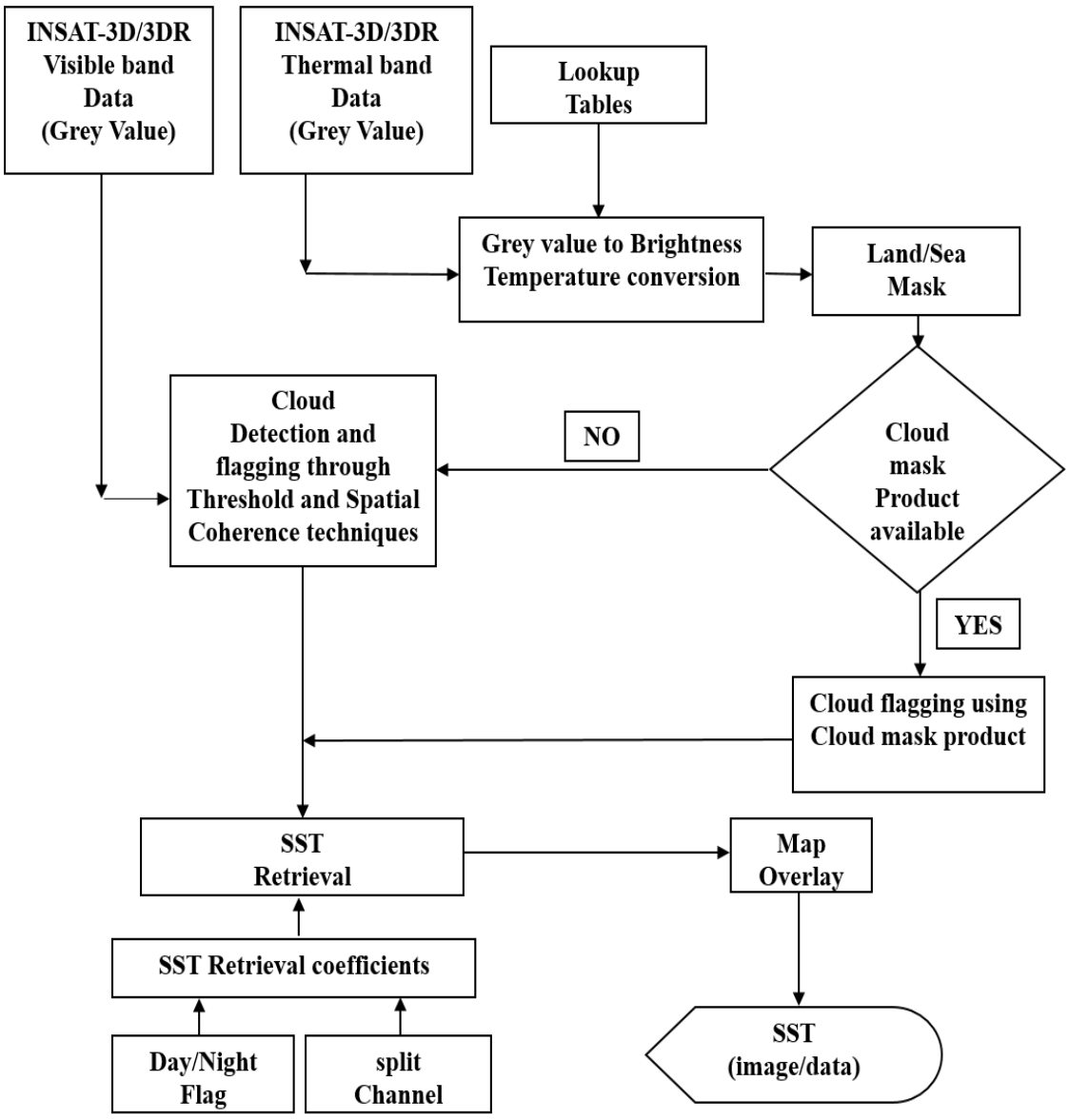

Fig. 3: Flow-chart of SST Retrieval from INSAT-3DR Imager

3.3 Operational Implementation

The implementation is done in the following steps:

Step-1. Reading of the grey counts, geolocation, satellite and solar zenith angles.

Step-2. Determine brightness temperatures from grey counts using the lookup table.

Step-3. Mask the land pixels using land/sea mask.

Step-4. Processing for discrimination between brightness temperatures from cloud free sea surface and those from the cloud tops as discussed in section 3.1.3.

Step-5. Computation of SST

For cloud-free pixels, SST is computed as

$$SST = a_0 + a_1T_1 + a_2(sec\theta - 1) + a_3T_{sfc}.(T_1 - T_2) + a_4(sec\theta - 1).(T_1 - T_2)$$

(a_0= 15.3364, a_1= 0.9535, a_2=- 0.8215, a_3= 0.0072, a_4=0.5144 for INSAT-3DR)

(a_0= 15.8150, a_1= 0.9519, a_2=- 0.8544, a_3= 0.0075, a_4=0.5340 for INSAT-3D)

where, *a's* and *b*'s are the retrieval coefficients, T_1, T_2 and T_3 are the brightness temperatures of TIR-1, TIR-2. T_{sfc} has been taken from the daily SST climatology.

Step-6. Quality control/Editing of derived SST

Only those SST values will be retained for which the following condition holds:

$$(SST_{clim} - 3\sigma) \leq SST \leq (SST_{clim} + 3\sigma)$$

where, σ is the standard deviation of the daily climatological SST and SST_{clim} is the daily value of climatological SST.

3.4 Output

SST maps and data (HDF5) are available every half hourly, daily, weekly, monthly and seasonally.

Parameter	Min (K)	Max (K)	Theoretical Accuracy	Resolution
SST(day)	285	310	~0.7-0.8 K (with 0.10-0.15 K noise)	Pixel (~4 km)

3.4.1 Format of the output and the domain

HDF5 data sets : Latitude, Longitude, SST, Quality flag

Domain : 40^0 S to 40^0 N, 30^0 E to 120^0 E

3.5 Validation

The extensive validation of the derived SST will be done using all the available data from buoys, special cruise by research vessels and available similar products from various satellite missions.

3.5.1 Initial validation

Preliminary validation of SST retrieved through the proposed algorithm for both INSAT-3D & 3DR with concurrent in-situ as well as MODIS/Aqua SST been performed for 11-18 December, 2017. Comparison of operational products have also been performed with same in-situ SST data for the same period. We have taken 0.04^0 spatial resolution and 15 minutes' temporal resolution for collocation. The daily products have also been compared with GHRSST (Group for High Resolution SST) daily SST products for the same period.

3.5.1.1 Comparison with in-situ:

The in situ records acquired from In-situ quality monitor (Iquam) portal hosted by National Oceanic and Atmospheric Administration (NOAA) are first temporally matched-up against the INSAT-3D/3DR extractions. To limit variability introduced by the time separation between the two data sources, the absolute difference between the time of the in situ SST measurement and the time at which that location is viewed by the INSAT-3D/3DR (i.e., the matchup time window) is restricted to a maximum of ±15 minutes. In situ records that do not fall within the stipulated time window will be rejected. The in situ records that pass the temporal matchup subsequently have to pass a spatial test.

The figures 4(a) and 4(b) are showing the scatter plot of INSAT-3D SST retrieved through new and operational algorithm with respect to concurrent in-situ SST measurements while figures 5(a) and 5(b) are showing the same for INSAT-3DR SST.

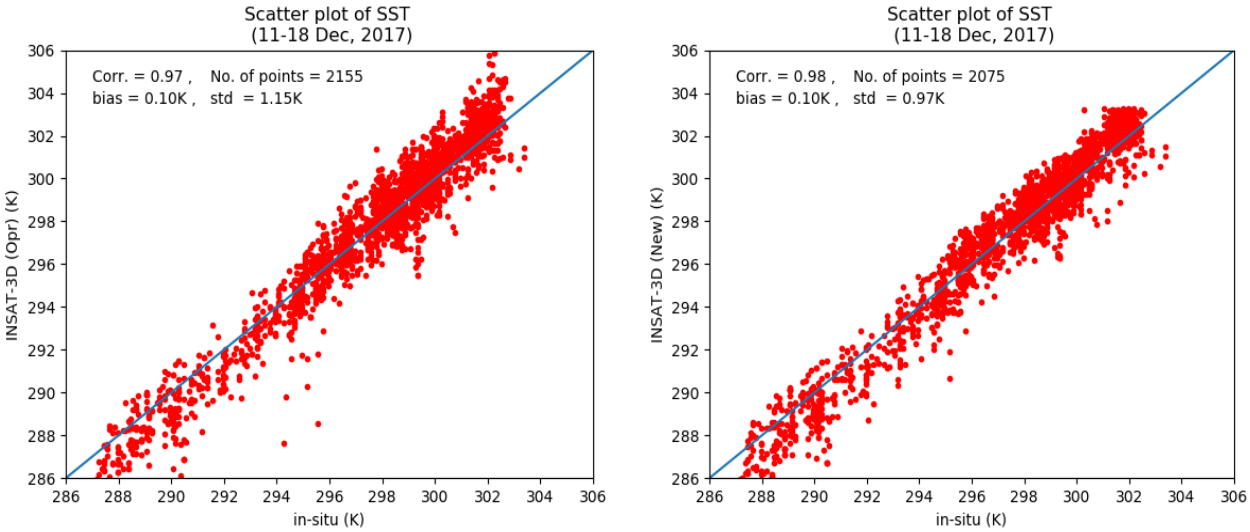

(a) (b)

Fig. 4: Scatter plot of INSAT-3D SST with in-situ SST (a) Operational (b) New

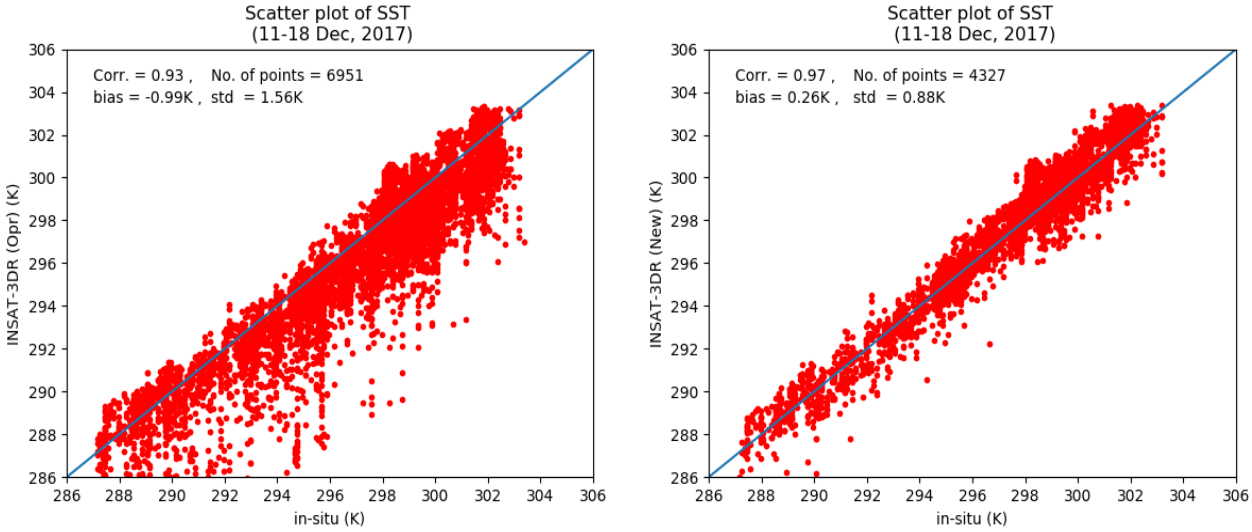

(a) (b)

Fig. 5: Scatter plot of INSAT-3DR SST with in-situ SST (a) Operational (b) New

From above figures (4) and (5), it can be seen that the spread is less in new SST as compared to operational SST when compared with same in-situ data for both satellites. This clearly indicates an improvement in SST when retrieved using proposed algorithm than the operational SST. The correlation coefficient also shows an improvement.

3.5.1.2 Comparison with MODIS/Aqua:

A preliminary comparison of SST retrieved using new as well as operational algorithm for both INSAT-3D & 3DR satellites has been carried out with MODIS/Aqua SST for the same period of 11-18, December 2017. Figures (6-7) are showing the density scatter plot for both the products: new as well as operational for both INSAT-3D and INSAT-3DR sensors.

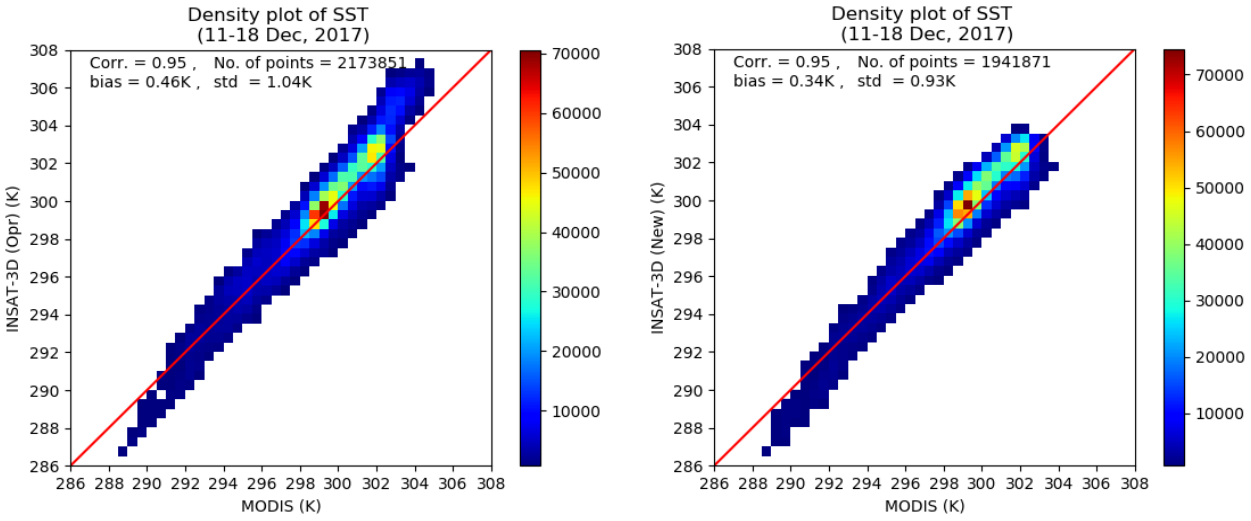

(a) (b)

Fig. 6: Density plot of retrieved INSAT-3D SST with MODIS (a) Operational (b) New SST

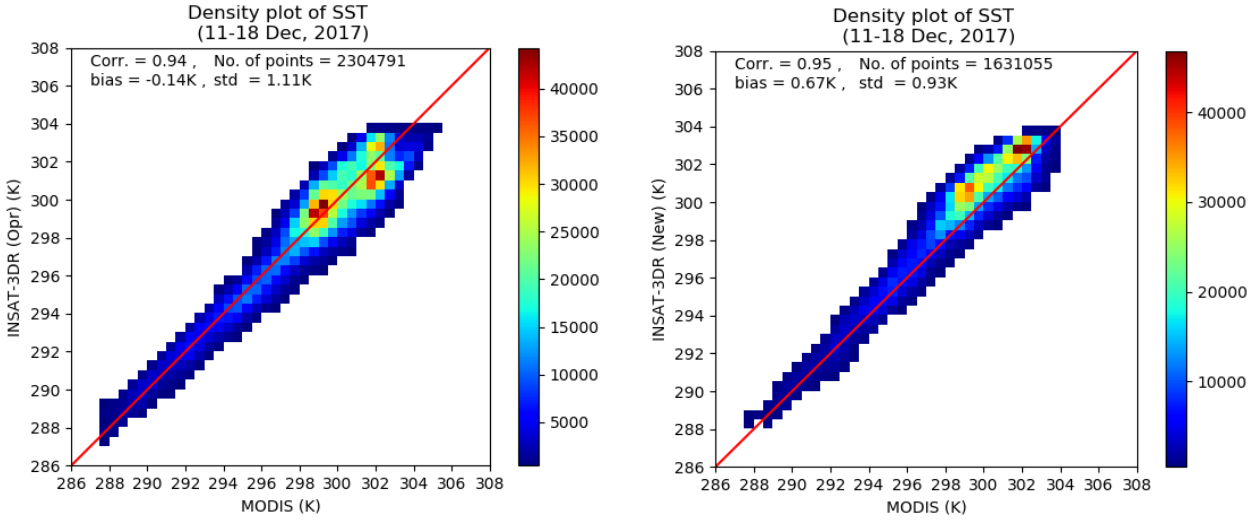

(a) (b)

Fig. 7: Density plot of retrieved INSAT-3D SST with MODIS (a) Operational (b) New

The quantitative comparison in terms of correlation coefficient, mean difference (bias), the standard deviation of the difference (Std) with respect to MODIS SST has also been shown in same figures. From the above figures it is clear that both the bias and Std of new SST are less than that of operational SST when compared with MODIS. Therefore, SST accuracy is improved when retrieved using the proposed algorithm.

3.5.2.3 Comparison with GHRSST DAILY Products:

An initial comparison of daily SST products retrieved using new as well as operational algorithm for both INSAT-3D & 3DR satellites has been carried out with GHRSST daily SST products for the same period of 11-18, December 2017. The comparison has been shown by the spatial plots of the differences in both the SST products. The following figures (8) and (9) are showing the spatial plots of the differences for INSAT-3D and INSAT-3DR, respectively for 11th December 2017.

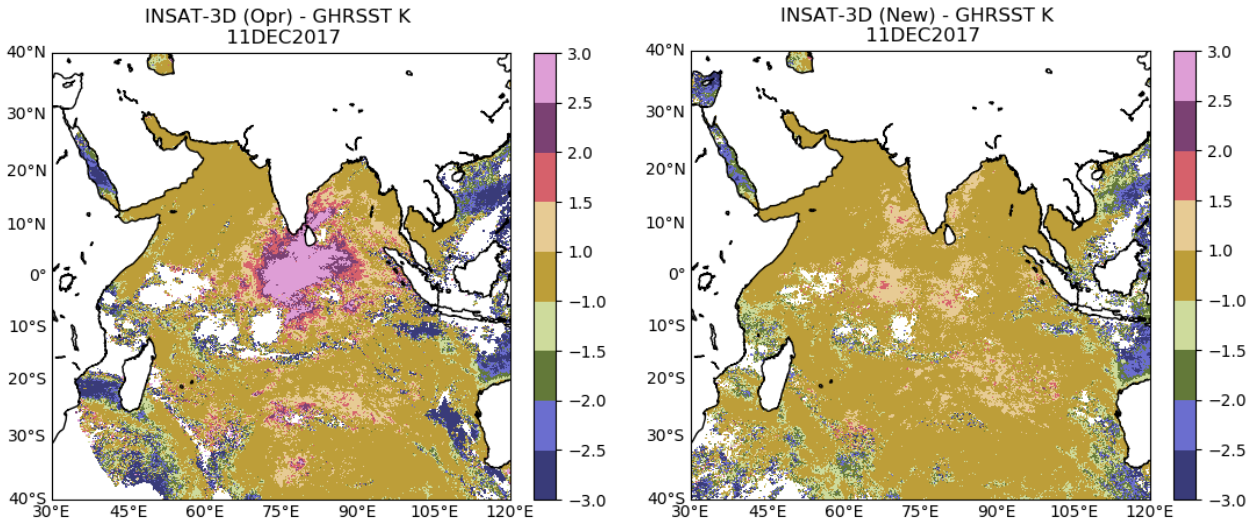

(a) (b)

Fig. 8: Difference of daily INSAT-3D SST with GHRSST (a) Operational (b) New

It can be clearly seen from the above figures (8) and (9) that except some locations the difference between INSAT-3D/3DR SST and GHRSST is within ±1K when retrieved through proposed algorithm. While the difference between operational SST and GHRSST products is as high as 2.5 to 3K in case of INSAT-3D and as low as -2.5 to -3K in case of INSAT-3DR. This clearly indicates the superiority of the proposed algorithm over the operational one.

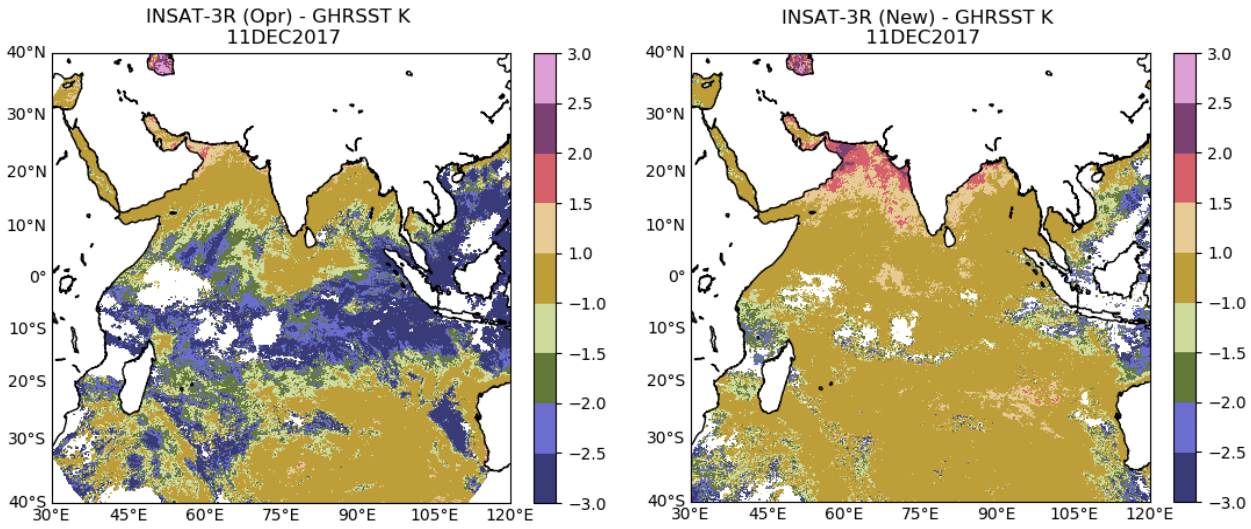

(a) (b)

Fig. 9: Difference of daily INSAT-3DR SST with GHRSST (a) Operational (b) New

3.6 Applications

There are many potential applications of SST. Among those thermal gradient is one of the most important features of the SST which is required to study various mesoscale oceanic processes as well as a serves as an indicator of potential fishery zones (PFZ). Thermal gradients from GHRSST daily products is shown in figure (10).

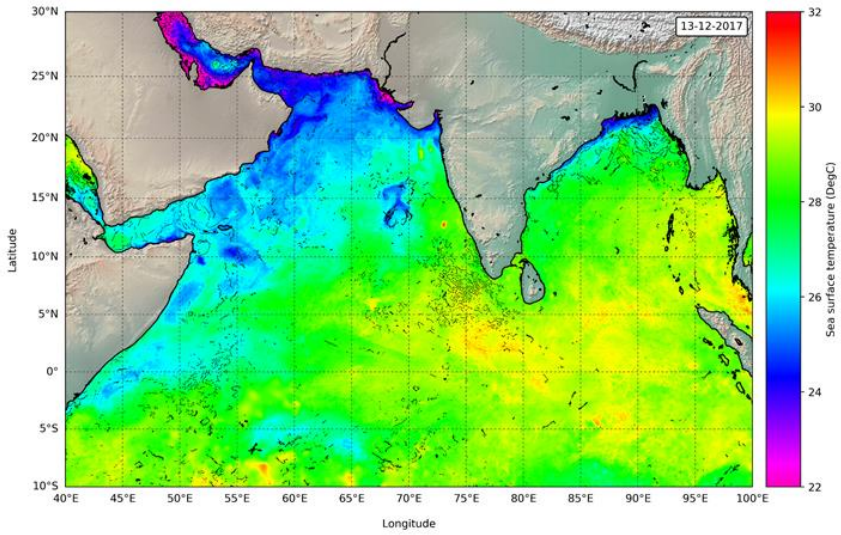

Fig. 10: Thermal gradient from daily GHRSST for 13th December 2017.

The thermal gradients computed from daily products of INSAT-3D/3DR SST retrieved through proposed and operational algorithm for 13th December 2017 are shown in the following figures (11) and (12). This work has been carried out with our colleagues from oceanic sciences division (OSD).

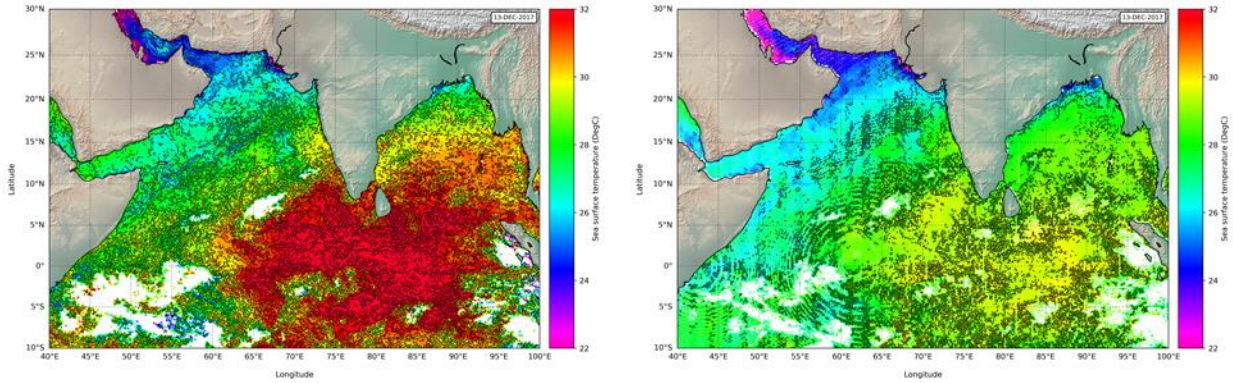

(a) (b)

Fig. 11: Thermal gradients from daily INSAT-3D SST (a) Operational (b) New

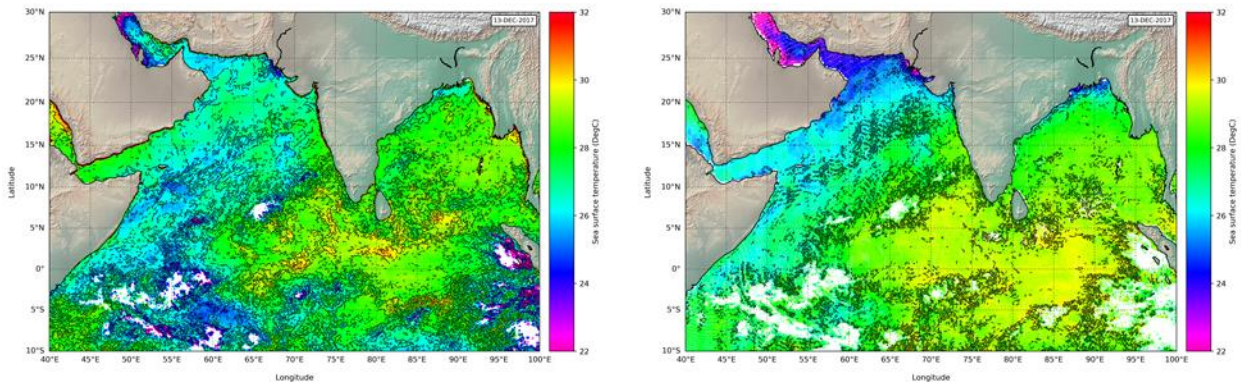

(a) (b)

Fig. 12: Thermal gradients from daily INSAT-3DR SST (a) Operational (b) New

On comparing figures (11) and (12) with figure (10), we can see that for both INSAT-3D & 3DR the SST gradients calculated from the daily SST products retrieved through proposed algorithm is closer to GHRSST gradients as compared to gradients calculated from SST retrieved through operational algorithm.

The above initial validation exercise confirms the superiority of the proposed algorithm over the operational one.

3.7 Technical issues (limitation etc.)

Accuracy of the product depends on the accuracy of the radiative transfer model to simulate the satellite radiances, instrument noise and atmospheric correction. Biases in radiative transfer model simulations can be accounted for by validating the derived SST with reliable and concurrent in-situ data. In the absence of split thermal window channel observations and a channel sensitive to intervening atmospheric total water vapour content, the atmospheric correction applied is an indirect. The accuracy of this correction will heavily depend upon the accuracy of the model reanalysis for total water vapour. Major constraints on data quality outside the scope of this effort focus in the following areas: accurate pre-launch instrument characterization, instrument NEΔT for each band, calibration model performance, availability of quality controlled surface calibration-validation observations, availability and access to the various quality assessment data sets, and timely access to continuing performance assessment data sets. The on-orbit instrument NEΔT performance is a primary input to the algorithm error budget.

3.7 Future Scope

Initially, this proposed algorithm and bias correction would be used to derive SST. Over a period of approximately one year, after complete calibration and validation of the product, bias correction and other fine tuning of the coefficients would be carried out. This should improve the accuracy of the product to the desired level. Of course, instrument noise also plays a crucial role in determining the overall accuracy of the product. Generation of regression coefficients for SST retrieval from simultaneous satellite and buoy observations data base require nearly 250 buoys distributed over Arabian Sea, Bay of Bengal and Indian Ocean continuously for minimum 2/3 years.

Moreover, the bias correction as mentioned above is based on the simulated brightness temperatures using ECMWF analysis profiles and PFAAST RT model. Also, ECMWF analysis profiles may also have some biases which can cause the biases in the simulated brightness temperatures. Therefore, in future we will refine this bias correction using radiosonde based atmospheric profiles. Similarly, RT models also known to have inherent biases. Hence, better RT model like OPTRON will also be explored to reduce the RT model biases.

References:

1 Ackerman Steve, Kathleen Strabala, Paul Menzel, Richard Frey, Chris Moeller, Liam Gumley, Bryan Baum, Suzanne Wetzel Seemann, and Hong Zhang (2006), "Discriminating Clear-sky from Cloud with MODIS Algorithm Theoretical Basis Document (MOD35)."

2 Anding D. and R. Kauth (1970), "Estimation of sea surface temperature from space," Remote Sensing of Environment, 1, 217-220.

3 Barton I. J., (1983), "Dual channel satellite measurements of sea surface temperature," Quarterly journal of Royal Meteorological Society, 109,365-378.

4 Barton, I. J., A. J. Prata, and D. T. Llewellyn-Jones, (1993), "The Along Track Scanning Radiometer–an Analysis of coincident ship and satellite measurements," Adv. Space Res., 13(5), 69.

5 Deschamps, P. Y. and T. Phulpin, (1980), "Atmospheric corrections of infrared measurements of sea surface temperature using channels at 3.7 μm, 11 μm and 12 μm." Boundary Layer Meteor. 18, 131-143.

6 Gohil B. S., A. K. Mathur and P. C. Pandey, (1994), "An algorithm for sea surface temperature estimation from ERS-1 ATSR using moisture dependent coefficients: a simulation study," International Journal of Remote Sensing, Vol. 15, No.5, 1161-1167.

7 Llewellyn-Jones, D.T., P.J. Minnett, R.W. Saunders and A.M. Závody, (1984), "Satellite multichannel infrared measurements of sea surface temperature of the N.E. Atlantic Ocean using AVHRR/2." Quart. J. R. Met. Soc. 110, 613-631.

8 Mathur A.K. and V.K. Agarwal, (1991), "A quantitative study on the effect of water vapour on estimation of sea surface temperature using satellite IR observations," Oceanography of the Indian Ocean, B. N. Desai, Ed., Oxford & IBH publishing Co. Pvt. Ltd., 673-680.

9 Mathur A. K., V. K. Agarwal and T. C. Panda, (2002), "Validation of ERS-1/ATSR derived SST in Indian waters," International Journal of Remote Sensing, Vol. 23, No. 24, 5155-5163 pp.

10 Minnett P. J., (1988), "Satellite Infrared Scanning Radiometers-AVHRR and ATSR/M, Microwave Remote Sensing for Oceanographic and Marine Weather-Forecast Models," edited by R. A. Vaughan, Kluwer Academic Publishers, Dordrecht.

11 Mutlow C. T., A. M. Zavody, I. J. Barton, and D. T. Llewellyn-Jones, (1994), "Sea surface temperature measurements by the along-track scanning radiometer on the ERS-1 satellite," Early results, *J. Geophys. Res*., **99**, 22575-22588.

12 Prabhakar C., G. Dalu and V. G. Kunde, (1974), "Estimation of Sea surface temperature from remote sensing in 11-13 μm window region," Journal of Geophysical research, 79, 5039-5044.

13 Shenoy S. C. (1999), "On the suitability of global algorithms for the retrieval of SST from the north Indian Ocean using NOAA/AVHRR data," International Journal of Remote Sensing, 20, 1, 11-29.

14 Walton, C. C., W. G. Pichel, and J. F. Sapper (1998), "The development and operational application of non-linear algorithms for the measurement of sea surface temperature s with the NOAA polar-orbiting environmental satellites," Journal of Geophys. Res.,103, 27,999-28,012.